DOI: 10.13009/EUCASS2019-229

DOI: 229

Multiphase Baer-Nunziato type models for the simulation of self-pressurizing tanks

M. Gandolfi[⋆] *and P. Barbante*[†]
[⋆]*Politecnico di Milano, DAER, Via A. La Masa 34, 20156 Milano, Italy*
[†]*Politecnico di Milano, Dept. of Mathematics, P.zza L. Da Vinci 32, 20133 Milano, Italy*
michele1.gandolfi@mail.polimi.it · paolo.barbante@polimi.it

Abstract

Self-pressurizing tank dynamics is modeled using a Baer-Nunziato type multiphase model, with relaxation source terms that account for the exchange of momentum, energy and matter among the phases. Numerical results for nitrous oxide are compared to experimental results available in literature. Since the source terms have an infinite relaxation speed, local thermodynamic equilibrium is reached and the model cannot reproduce the initial pressure and temperature drop observed in experimental results. However it well approximates the subsequent linear decrease of pressure with respect to time. Future work will investigate the effects of finite relaxation speed of the source terms.

1. Introduction

Nitrous oxide (N_2O) is one of the liquid oxidizers used in hybrid rockets because it is storable at room temperature, it is easy to handle since it does not need thermal control, it is non-toxic, its critical temperature is close to ambient temperature and has an high vapor pressure. This means that nitrous oxide vapor can be used as the pressurant of the tank and so pumps, complex plumbing and external pressurization systems are not required making the propulsion system simpler and lighter. This kind of tanks are called self-pressurizing tanks. When a self-pressurizing tank is drained, phenomena such as phase transition and heat transfer between liquid and vapor occur. If these aspects are not modeled accurately pressure history inside the tank and also mass flow rate out of the tank can not be predicted. Nowadays self-pressurizing tanks dynamic is described using zero dimensional models of various complexity.[15] The purpose of this article is to apply a new model to this problem. The tank geometry will be one-dimensional, even tough the model examined here can simulate three dimensional tanks. Moreover since this is the first time that this model is applied to a self-pressurizing tank, heat transfer from the fluid to the tank walls and from these to the surroundings is not taken into account for the sake of simplicity.

2. Multicomponent model

The multicomponent Baer-Nunziato[2] type model used in this work is an adaptation of the work of Han et al.,[5] itself an extension of the one originally developed by Saurel and Abgrall.[9] It is a non-equilibrium model where each component $k = 1, \dots, K$ has its own density ρ_k, velocity $\boldsymbol{v}_k$ pressure p_k, internal energy e_k and volume fraction α_k. Chemical species and phases are components, i.e. if the same chemical species is found in two phases we count two components. In Baer-Nunziato type models the interface between phases is not tracked explicitly and the amount of each phase is determined by the volume fraction α_k. Volume fractions obey a saturation constraint that reads:

$$\sum_{k=1}^{K} \alpha_k = 1, \qquad \alpha_k \in [0, 1] \tag{1}$$

The evolution of volume fractions is governed by:

$$\frac{\partial \alpha_k}{\partial t} + \boldsymbol{V}_I \cdot \nabla \alpha_k = S_{\alpha,k}(\boldsymbol{w}), \quad k \in \{1, \dots, K-1\} \tag{2}$$

DOI: 10.13009/EUCASS2019-229

where $\boldsymbol{V}_I$ is the interfacial velocity. One of the volume fractions, e.g. α_K, can be obtained from the saturation constraint:

$$\alpha_K = 1 - \sum_{k=1}^{K-1} \alpha_k. \tag{3}$$

The fluid equations for each component are:

$$\frac{\partial \boldsymbol{u}_k}{\partial t} + \nabla \cdot (\boldsymbol{f}_k(\alpha_k, \boldsymbol{u}_k)) = \boldsymbol{H}(\boldsymbol{w})\nabla\alpha_k + \boldsymbol{S}_{\boldsymbol{u},k}(\boldsymbol{w}), \quad k \in \{1, \cdots, K\} \tag{4}$$

where:

$$\boldsymbol{u}_k \coloneqq \begin{bmatrix} \alpha_k\rho_k \\ \alpha_k\rho_k\boldsymbol{v}_k \\ \alpha_k\rho_k E_k \end{bmatrix}, \quad \boldsymbol{f}_{k,i} \coloneqq \begin{bmatrix} \alpha_k\rho_k v_{k,i} \\ \alpha_k\rho_k v_{k,i}\boldsymbol{v}_k + \alpha_k p_k \boldsymbol{e}_i \\ \alpha_k\rho_k v_{k,i}\left(E_k + \frac{p_k}{\rho_k}\right) \end{bmatrix}, \tag{5}$$

$$\boldsymbol{H} \coloneqq \begin{bmatrix} \boldsymbol{0}^T \\ P_I \boldsymbol{I}_{dxd} \\ P_I \boldsymbol{V}_I^T \end{bmatrix}, \quad \boldsymbol{S}_{\boldsymbol{u},k} \coloneqq \begin{bmatrix} S_{\rho,k} \\ \boldsymbol{S}_{\rho\boldsymbol{v},k} \\ S_{\rho E,k} \end{bmatrix}, \tag{6}$$

$$\boldsymbol{w} \coloneqq \begin{bmatrix} \boldsymbol{\alpha}^T \\ \boldsymbol{u}_1^T \\ \vdots \\ \boldsymbol{u}_K^T \end{bmatrix}, \quad \boldsymbol{\alpha} \coloneqq \begin{bmatrix} \alpha_1 \\ \vdots \\ \alpha_K \end{bmatrix}, \tag{7}$$

and $\boldsymbol{e}_i$ and $\boldsymbol{I}_{dxd}$ represent the *i-th* unit vector in $\mathbb{R}^d$ and the identity matrix in $\mathbb{R}^{dxd}$ respectively. These equations are the Euler equations with the addition of source terms that account for the exchange of mass, momentum and energy among components. Also an equation of state for each component, such as Eq. 41 described in Sec. 3, must be introduced. Effects due to gravity, heat transfer from fluid to tank walls and from these to the surroundings, surface tension and viscosity are neglected in the equations written above, however they can be easily added. E_k is the specific total energy and it is equal to $e_k + \boldsymbol{v}_k^T\boldsymbol{v}_k/2$. P_I is the interfacial pressure. Interfacial pressure P_I and interfacial velocity $\boldsymbol{V}_I$ are defined in the following way:

$$P_I \coloneqq \sum_{k=2}^{K} p_k \quad \text{and} \quad \boldsymbol{V}_I \coloneqq \boldsymbol{v}_1 \tag{8}$$

This choice is in agreement with the second law of the thermodynamics as proved in Müller et al.[6] Since a relaxation procedure towards equilibrium will be applied, a different numbering of the components would provide the same results. In this non equilibrium model the various components can have different velocities, pressures, temperatures and chemical potentials μ_k in the same point. Source terms, denoted with S, on the right hand side of Eqs. 2, 4 describe mass, momentum and energy transfer between the components via velocity, pressure, temperature and chemical potential relaxation. Relaxation drives velocity, pressure, temperature and chemical potential of the various components, towards local mechanical and thermodynamic equilibrium. Definitions of source terms in Eqs. 2, 4 can be found in Han et al.[5] and Zein.[13]

In order to discretize the coupled system of Eqs. 2 and 4 a Strang operator splitting is performed[11,12] resulting in the following system of equation of fluid motion:[5,9]

$$\frac{\partial \alpha_k}{\partial t} + \boldsymbol{V}_I \cdot \nabla\alpha_k = 0, \quad k \in \{1, \ldots, K-1\} \tag{9}$$

$$\frac{\partial \boldsymbol{u}_k}{\partial t} + \nabla \cdot (\boldsymbol{f}_k(\alpha_k, \boldsymbol{u}_k)) = \boldsymbol{H}(\boldsymbol{w})\nabla\alpha_k, \quad k \in \{1, \ldots, K\} \tag{10}$$

and the relaxation system:

$$\frac{d\alpha_k}{dt} = S_{\alpha,k}(\boldsymbol{w}), \quad k \in \{1, \ldots, K-1\}, \tag{11}$$

$$\frac{d\boldsymbol{u}_k}{dt} = \boldsymbol{S}_{\boldsymbol{u},k}(\boldsymbol{w}), \quad k \in \{1, \ldots, K\}. \tag{12}$$

Eqs. 9 and 10 represent fluid evolution in time and space, whereas Eqs. 11 and 12 describes an evolution in time only, for a fixed position in space. Integration of Eqs. 11 and 12 can be replaced by the relaxation procedures, performed at each time step, that will be described in Sec. 2.2.

DOI: 10.13009/EUCASS2019-229

2.1 Finite volume scheme

Equations 9 and 10 are solved using a finite volume scheme that makes use of an upwind discretization: the scheme preserves homogeneous pressure and velocity fields.[4,5] The resulting scheme is:

$$(\alpha_k)_i^{n+1} = (\alpha_k)_i^n - \frac{\Delta t}{|V_i|} \sum_{j \in \mathcal{I}(i)} |\Gamma_{ij}| (\bar{\boldsymbol{V}}_I)_{ij} \cdot (\nabla \alpha_k)_{ij}^n, \tag{13}$$

$$(\boldsymbol{u}_k)_i^{n+1} = (\boldsymbol{u}_k)_i^n - \frac{\Delta t}{|V_i|} \sum_{j \in \mathcal{I}(i)} |\Gamma_{ij}| \boldsymbol{G}_{ij}^n, \tag{14}$$

where i represents the *i-th* cell, n represents the time step level, $|V_i|$ represents the volume of cell i, $|\Gamma_{ij}|$ is the area of the interface between cells i and j and the set $\mathcal{I}$ is composed by the neighbor cells. The fluxes $\boldsymbol{G}_{ij}^n$ are defined as:

$$\boldsymbol{G}_{ij}^n \coloneqq \boldsymbol{F}_k(\boldsymbol{w}_{ij}^n, \boldsymbol{w}_{ji}^n, \boldsymbol{n}_{ij}) - \boldsymbol{H}(\bar{\boldsymbol{w}}_{ij})(\nabla \alpha_k)_{ij}^n, \tag{15}$$

$$\boldsymbol{F}_k(\boldsymbol{w}_{ij}^n, \boldsymbol{w}_{ji}^n, \boldsymbol{n}_{ij}) \coloneqq \sum_{l=1}^{d} \boldsymbol{f}_{k,l}(\bar{\boldsymbol{w}}(\boldsymbol{w}_{ij}, \boldsymbol{w}_{ji}))(\boldsymbol{n}_{ij})_l, \tag{16}$$

$$(\nabla \alpha_k)_{ij}^n \coloneqq ((\bar{\alpha}_k)_{ij} - (\alpha_k)_i^n)\boldsymbol{n}_{ij}. \tag{17}$$

This discretization is not conservative, in fact the flux that leaves a cell through one of its interfaces, in general is different form the flux that enters a neighboring cell through the same interface. This is the effect of the presence of the term $(\bar{\boldsymbol{V}}_I)_{ij} \cdot (\nabla \alpha_k)_{ij}$ in Eq. 13 and of the term $\boldsymbol{H}(\bar{\boldsymbol{w}}_i j)(\nabla \alpha_k)_{ij}$ in the definition of the fluxes of Eq. 15, since the gradient of the volume fractions can have different values in two neighboring cells. Quantities $(\bar{\alpha}_k)_{ij}$, $(\bar{\boldsymbol{V}}_I)_{ij}$ and $\bar{\boldsymbol{w}}_{ij}$ are evaluated solving a Riemann problem at cell interface Γ_{ij}. The flux at cell interface is then computed in two steps:

1. reconstruct $\rho_k, \boldsymbol{v}_k, p_k$ and volume fractions α_k at cell interface to obtain left and right states $\boldsymbol{w}_{ij}$ and $\boldsymbol{w}_{ji}$ at cell interface,

2. solve the multi-phase, multi-component Riemann problem determined by $\boldsymbol{w}_{ij}$ and $\boldsymbol{w}_{ji}$ at each cell interface. In this work this is achieved using the HLLC Riemann solver.[4]

2.2 Relaxation procedures

The main assumption is that the relaxation velocity of the source terms is infinite, thus mechanical and thermodynamic equilibrium will be locally reached at each time step. Starting from the relaxation system (Eqs. 11 and 12), summing over all equations and making use of the following constraints on the source terms:

$$\sum_{k=1}^{K} S_{\alpha,k}^{\xi} = 0, \quad \sum_{k=1}^{K} S_{\rho,k}^{\xi} = 0, \quad \sum_{k=1}^{K} \boldsymbol{S}_{\rho \boldsymbol{v},k}^{\xi} = 0, \quad \sum_{k=1}^{K} S_{\rho E,k}^{\xi} = 0, \tag{18}$$

one obtains:

$$\sum_{k=1}^{K} \frac{d\alpha_k}{dt} = 0, \quad \frac{d\rho}{dt} = 0, \quad \frac{d(\rho \boldsymbol{v})}{dt} = \boldsymbol{0}, \quad \frac{d(\rho E)}{dt} = 0, \tag{19}$$

where ρ, $\rho \boldsymbol{v}$ and ρE are respectively mixture density, mixture momentum and mixture total energy. They are defined as:

$$\rho \coloneqq \sum_{k=1}^{K} \alpha_k \rho_k, \quad \rho \boldsymbol{v} \coloneqq \sum_{k=1}^{K} \alpha_k \rho_k \boldsymbol{v}_k, \quad \rho E \coloneqq \sum_{k=1}^{K} \alpha_k \rho_k E_k \tag{20}$$

This means that during the relaxation procedure mixture density, momentum, total energy and velocity remain constant. Now the relaxation procedures,[5] that enforce local mechanical and thermodynamic equilibrium, will be shortly described.

DOI: 10.13009/EUCASS2019-229

2.2.1 Velocity relaxation procedure

The velocity relaxation procedure can be summarized as follows:

1. update the velocity of each component using:

$$\boldsymbol{v}_k^{\infty} = \boldsymbol{v}^{\infty} = \boldsymbol{v}^0 = \frac{\sum_{k=1}^{K}(\alpha_k^0 \rho_k^0 \boldsymbol{v}_k^0)}{\sum_{k=1}^{K} \alpha_k^0 \rho_k^0}, \tag{21}$$

2. update the total energy of each component using:

$$E_k^{\infty} = E_k^0 + \boldsymbol{v}^0(\boldsymbol{v}^0 - \boldsymbol{v}_k^0). \tag{22}$$

where 0 refers to the condition before the relaxation and ∞ refers to the condition after the relaxation.

2.2.2 Simultaneous pressure and temperature relaxation

The simultaneous pressure and temperature relaxation procedure[5] is modified in order to use the Noble-Abel Stiffened Gas (NASG) equation of state. As in the velocity relaxation procedure, it is assumed that the relaxation process is infinitely fast and that the solution of the ODEs system converges towards the equilibrium state where:

$$p_k^{\infty} = p^{\infty}, \quad T_k^{\infty} = T^{\infty}, \tag{23}$$

and since the source terms related to pressure and temperature relaxation in the mass and momentum equations of system 12 are equal to zero:

$$\alpha_k^{\infty} \rho_k^{\infty} = \alpha_k^0 \rho_k^0, \tag{24}$$

$$\boldsymbol{v}_k^{\infty} = \boldsymbol{v}_k^0. \tag{25}$$

During this relaxation procedure the mixture internal energy is preserved:

$$\sum_{k=1}^{K}(\alpha_k \rho_k e_k)^{\infty} = \sum_{k=1}^{K}(\alpha_k \rho_k e_k)^0, \tag{26}$$

combining Eq. 26, Eq. 24 and the NASG-EOS (Eq. 41) one obtains:

$$\lambda := \sum_{k=1}^{K} \alpha_k^0 \frac{p_k^0 + \gamma_k \pi_k}{\gamma_k - 1}(1 - \rho_k^0 b_k). \tag{27}$$

Defining:

$$B_k = (\alpha\rho)_k^0 b_k, \tag{28}$$

and:

$$C = 1 - \sum_{k=1}^{K} B_k, \tag{29}$$

and imposing temperature equilibrium at the end of the relaxation procedure ($T_k^{\infty} = T^{\infty}$), with the use of Eq. 43 it is possible to find the following expression for α_k^{∞}:

$$\alpha_k^{\infty} = \alpha_{k_0}^0 \frac{a_k}{a_{k_0}} \frac{p^{\infty} + \pi_{k_0}}{p^{\infty} + \pi_k} + B_k - \frac{a_k}{a_{k_0}} \frac{p^{\infty} + \pi_{k_0}}{p^{\infty} + \pi_k} B_{k_0}, \tag{30}$$

where k_0 is a reference component and a is defined as:

$$a_k := c_{v,k}(\gamma_k - 1)\alpha_k^0 \rho_k^0. \tag{31}$$

DOI: 10.13009/EUCASS2019-229

Using Eqs. 1 and 30 it is possible to obtain $\alpha^{\infty}_{k_0}$ as:

$$\alpha^{\infty}_{k_0} = \frac{C}{\sum_{k=1}^{K} \frac{a_k}{a_{k_0}} \frac{p^{\infty} + \pi_{k_0}}{p^{\infty} + \pi_k}} + B_{k_0}. \tag{32}$$

Introducing the sets:

$$\mathcal{E} := \{k : \pi_k = \pi_{k_0}, k \in \{1, \dots, K\}\}, \quad \mathcal{N} := \{k : \pi_k \neq \pi_{k_0}, k \in \{1, \dots, K\}\},$$

replacing Eq. 32 into Eq. 30 and sticking everything into Eq. 27, one gets the following equation where the only unknown is p^{∞}:

$$\begin{aligned} &\sum_{k \in \mathcal{E}} \frac{a_k}{a_{k_0}} \left(\frac{p^{\infty} + \gamma_k \pi_k}{\gamma_k - 1} - \frac{\lambda}{C} \right) \prod_{l \in N} (p^{\infty} + \pi_l) + \\ &+ \sum_{k \in \mathcal{N}} \frac{a_k}{a_{k_0}} \left(\frac{p^{\infty} + \gamma_k \pi_k}{\gamma_k - 1} - \frac{\lambda}{C} \right) (p^{\infty} + \pi_{k_0}) \prod_{l \in \mathcal{N}, l \neq k} (p^{\infty} + \pi_l) = 0, \end{aligned} \tag{33}$$

Equilibrium pressure p^{∞} is the root of Eq. 33, a polynomial of degree $\mathcal{N} + 1$. The only physical solution is the one that satisfies $p^{\infty} > 0$ and $0 \leq \alpha^{\infty}_k \leq 1$. Reference phase k_0 has to be chosen such that the cardinality of $\mathcal{N}$ is the lowest. Finally the equilibrium temperature can be computed using:

$$T^{\infty}_k = T^{\infty} = C \left(\sum_{l=1}^{K} \frac{a_l}{p^{\infty} + \pi_l} \right)^{-1}. \tag{34}$$

Finally, knowing equilibrium pressure and temperature, ρ^{∞}_k and e^{∞}_k can be computed.

2.2.3 Chemical potential relaxation procedure

The chemical potential relaxation procedure will be now described. The starting point are the results obtained from the previous procedures, so p^0, T^0 and $\boldsymbol{v}^0$ are equal for all components. Velocity is not affected by the relaxation of chemical potentials. Furthermore it is assumed that, at the end of this procedure p^{∞} and T^{∞}, are the same for every component. For a two components system, like the one studied in this contribution, it is possible to define the following quantities:

$$\alpha^{\infty}_1 \rho^{\infty}_2 + \alpha^{\infty}_2 \rho^{\infty}_2 = \alpha^0_1 \rho^0_2 + \alpha^0_2 \rho^0_2 =: W \tag{35}$$

and

$$\sum_{k=1}^{2} \alpha^{\infty}_k \rho^{\infty}_k e^{\infty}_k = \sum_{k=1}^{2} \alpha^0_k \rho^0_k e^0_k =: E. \tag{36}$$

Phase equilibrium is reached when the chemical potentials of vapor (subscript 1) and liquid (subscript 2) are equal. Considering the following function:

$$f_{\mu}(\alpha_1 \rho_1) = \mu^{\infty}_1(\alpha_1 \rho_1) - \mu^{\infty}_2(\alpha_1 \rho_1), \tag{37}$$

it is possible to outline two situations.

1. For condensation $f_{\mu}(\alpha^0_1 \rho^0_1) > 0$, so $\alpha_1 \rho_1$ has to decrease. Since the numerical solutions requires, for numerical stability, that each component has to be present in all the domain, the smallest value for $\alpha_1 \rho_1$ is $\alpha^{\star}_1 \rho^{\star}_1 = tol$. The properties of each component are computed using p and T from the simultaneous pressure-temperature relaxation procedure, along with $\alpha^{\star}_1 \rho^{\star}_1$ and $\alpha^{\star}_2 \rho^{\star}_2 = W - \alpha^{\star}_1 \rho^{\star}_1$. If $f_{\mu}(\alpha^{\star}_1 \rho^{\star}_1) > 0$ total condensation occurs and the result of this procedure are the values of pressure, temperature, density obtained using $\alpha^{\star}_1 \rho^{\star}_1$. If $f_{\mu}(\alpha^0_1 \rho^0_1) < 0$ partial condensation occurs and it is possible to compute a root of f_{μ} in the interval $[\alpha^{\star}_1 \rho^{\star}_1, \alpha^0_1 \rho^0_1]$, using for example the bisection method.

DOI: 10.13009/EUCASS2019-229

2. For evaporation $f_\mu(\alpha_1^0\rho_1^0) < 0$, so $\alpha_1\rho_1$ has to increase. The maximum value that $\alpha_1\rho_1$ can achieve can be evaluated using:

$$\alpha_1^*\rho_1^* = \min\left(W - tol, \frac{E - Wq_2}{q_1 - q_2}\right), \tag{38}$$

where q_1 and q_2 are parameters of the NASG equation of state. If $f_\mu(\alpha_1^\star\rho_1^\star)$ is still negative, then total evaporation occurs; otherwise partial evaporation occurs and the root of f_μ can be found applying the bisection method in the interval $[\alpha_1^0\rho_1^0, \alpha_1^*\rho_1^*]$.

2.3 Outlet flow model

An injector is usually placed at the outlet of a self-pressurizing tank and its properties influence the tank dynamics. We compute the flow rate through the injector with the Dyer model,[3] as corrected by Solomon.[10] This model uses a weighted average of the rates produced by the single phase incompressible (SPI) model and the homogeneous equilibrium (HEM) model. The SPI model is accurate when fluid residence time inside the injector is much smaller than bubble growth time, i.e. there is not enough time for heat and mass transfer between the two phases to take place. The HEM model, on the opposite, is accurate when there is sufficient time for phase transition and for obtaining local equilibrium between phases. The SPI model computes mass flow rate G as:

$$G_{SPI} = C_d\sqrt{2\rho_1(p_1 - p_2)}, \tag{39}$$

where subscripts 1 and 2 refers to conditions upstream and downstream of the injector respectively, p and ρ are mixture properties and C_d is the injector discharge coefficient. The HEM model considers an isoentropic expansion in the injector and computes mass flow rate as:

$$G_{HEM} = C_d\rho_2\sqrt{2(h_1 - h_2)}, \tag{40}$$

where h is the mixture enthalpy.

3. Equation of state

The expression of thermodynamic properties according to the NASG-EOS is as follows:[7]

$$p(e, v) = (\gamma - 1)\frac{e - q}{v - b} - \gamma\pi \tag{41}$$

$$h(p, T) = C_pT + bp + q, \tag{42}$$

$$v(p, T) = \frac{(C_p - C_v)T}{p + \pi} + b, \tag{43}$$

$$s(p, T) = C_v\ln\frac{T^\gamma}{(p + \pi)^{\gamma-1}} + q', \tag{44}$$

$$g(p, T) = (\gamma C_v - q')T - C_vT\ln\frac{T^\gamma}{(p + \pi)^{\gamma-1}} + bp + q, \tag{45}$$

where p is the pressure, h the enthalpy, v the specific volume, s the entropy and g the Gibbs free energy. The sound speed is defined by:

$$c^2 = \frac{\gamma v^2(p + \pi)}{v - b}, \tag{46}$$

C_p is the specific heat at constant pressure, C_v the specific heat at constant volume, γ the specific heats ratio, b the covolume. The NASG-EOS is simple and contains the main properties of dense fluids such as thermal agitation through the term $(\gamma - 1)(e - q)$, molecular attractive effect, granting matter cohesion in condensed states through the therm $\gamma\pi$ and repulsive short distance effects through the term $v - b$. Parameters $\gamma, C_v, C_p, \pi, q, q', b$ are different for liquid and vapor since each phase has its own equation of state. Parameters are computed according to the procedure describe by Le Métayer,[7] with the difference that we compute the parameter π taking a minimum of the function:

$$f(\pi) = \sum_{i=1}^{N}\left(c_{i,exp}^2 - \frac{C_p(p_{i,exp} + \pi)v_{i,exp}^2}{v_{i,exp} - b}\right)^2, \tag{47}$$

DOI: 10.13009/EUCASS2019-229

Table 1: Vapor NASG EOS parameters

Temperature interval [K]	γ	π [Pa]	q [J/kg]	q' [J/(kgK)]	b [m^3/kg]	C_v [J/(kgK)]
270-295	2.303	5.454e+6	-1.734e+5	1.001e+4	-0.03	1.071e+3
260-285	1.948	2.52e+6	6.854e+4	4.432e+3	-0.023	7.522e+2
185-250	1.502	5.836e+3	2.673e+5	1.239e+3	-0.008	3.910e+2

Table 2: Liquid NASG EOS parameters

Temperature interval [K]	γ	π [Pa]	q [J/kg]	q' [J/(kgK)]	b [m^3/kg]	C_v [J/(kgK)]
270-295	2.83	1.634e+8	-5.345e+5	1.782e+4	-0.002	9.117e+2
260-285	2.505	1.93e+8	-4.524e+5	1.404e+4	-7.989e-4	9.073e+2
185-250	1.964	3.244e+8	-3.315e+5	7.874e+3	3.033e-4	9.112e+2

instead of computing it from a reference condition. The properties of N_2O used in the fitting are taken from the NIST database.[1] Tables 1 and 2 show NASG-EOS parameters for nitrous oxide in three different temperature intervals. In particular, the interval $185 - 250\,K$ is used to compute N_2O properties downstream of the injector in the Dyer model, while the other two intervals are used to compute N_2O properties inside the tank, for different initial conditions. Note that the parameter b, that represents the covolume, is negative for both phases in the first two temperature intervals of Tables 1 and 2 and only for vapor in the last temperature interval. In principle the covolume is a positive quantity, however here b is considered only as a fitting parameter and the negative value is accepted because it provides a good fitting of the experimental data. In the computation of the parameter π a local minimum of Eq. 47 was chosen instead of the global minimum (π of the order of $10^7\,Pa$), because the specific volume computed using the global minimum was constant with respect to temperature, in contrast with experimental results and the sound speed, computed with Eq. 46, does not change significantly using the local minimum instead of the global minimum. NASG equation of state provides a good estimation of most of the thermodynamic properties of liquid and gaseous nitrous oxide. Sound speed is poorly approximated by this equation of state in the temperature ranges presented in Tables 1 and 2, however this is not an issue for the computations performed in this work because the Mach number inside the tank is much smaller than one.

4. Results

The initial condition used in the computations match the experimental results[15] and are reported in Table 3. As initial condition it is assumed that liquid and vapor are saturated, with the pressure measured at the beginning of the experiments. The initial temperature is computed from the initial pressure. In each computation the domain is divided in two sections according to the tank fill level. The initial liquid volume fraction present in the tank ullage is set to 10^{-8} and the initial vapor volume fraction present in the part of the tank containing liquid is set to 10^{-8}. This choice stems from the fact that the multicomponent model requires, for numerical stability, to model the fluid as a mixture of all the components in the entire computational domain. The tolerance for the bisection method used in the chemical potential relaxation algorithm of Sec. 2.2 is 10^{-8} and the tolerance value of $\alpha_1\rho_1$ in the same procedure is 10^{-8}. Courant number is 0.3 in all the computations. The value of the injector discharge coefficient multiplied by the injector area, C_dA, is chosen so that experimental and computed pressure values are close to each other, as done also by Cantwell.[15] The outlet mass flow rate is computed with the Dyer model. On the other side of the domain, that corresponds to the close end of the tank, a wall boundary condition is applied. In all the computations a uniform grid is used. The computational domain length is different for each data set; so in order to have similar cells length in all the computations, the number of cells used to discretize the domain varies. The number of cells used is: 235 for Prince data set computation, 100 for Zimmerman data set computation, 400 for Zilliac data set computation.

Table 3: Initial data

Data set	Fill level [%]	p_i [MPa]	T_i [K]	v_i [m/s]	C_dA [m^2]	Final time [s]	Initial α
Prince	95	4.777	290.896	0	$23.6 * 10^{-6}$	5.56	10^{-8}
Zimmerman	87	3.763	280.758	0	$0.5875 * 10^{-6}$	4.86	10^{-8}
Zilliac	64	4.502	288.312	0	$83.25 * 10^{-6}$	4.91	10^{-8}

Tables 1 and 2 of Sec. 3 report the parameters used in the equations of state. Prince's and Zilliac's data sets computations use the $270 - 295\,K$ interval parameters, while Zimmerman's data set uses the $260 - 285\,K$ interval parameters since

DOI: 10.13009/EUCASS2019-229

the initial pressure and temperature are lower than in the other two cases.

4.1 Prince

Figures 1 and 2 show the results obtained using Prince's initial data. Initial conditions come from a hot flow test described in Prince et al.[8] The mean experimental pressure downstream of the injector was approximately 1.6 MPa, so this is the value taken as downstream pressure in the computations. Comparing the experimental and the computed pressure in Fig. 1(a), it is possible to notice that the latter shows an almost linear decrease of pressure with respect to time and does not have an initial pressure drop. This can be explained by the fact that in the multicomponent model used in this work, thermodynamic equilibrium is always reached locally in each cell at every time step, because the source terms relaxation velocity is infinite, thus transient behavior like the steep initial decrease of pressure can not be approximated. On the contrary, the linear decrease of pressure in the experimental results is well approximated by this model. Computed temperature in Fig. 1(b) shows the same trend of pressure. Another thing to notice is that pressure and temperature are uniform across the computational domain: this is due to the fact that the domain is short and the Mach number much smaller than one, so pressure waves travel in the computational domain fast enough to keep pressure uniform. Temperature is uniform too because of the infinite speed of relaxation and the local thermodynamic equilibrium. Figure 2 shows vapor and liquid volume fractions in selected cells plotted versus time. At the beginning

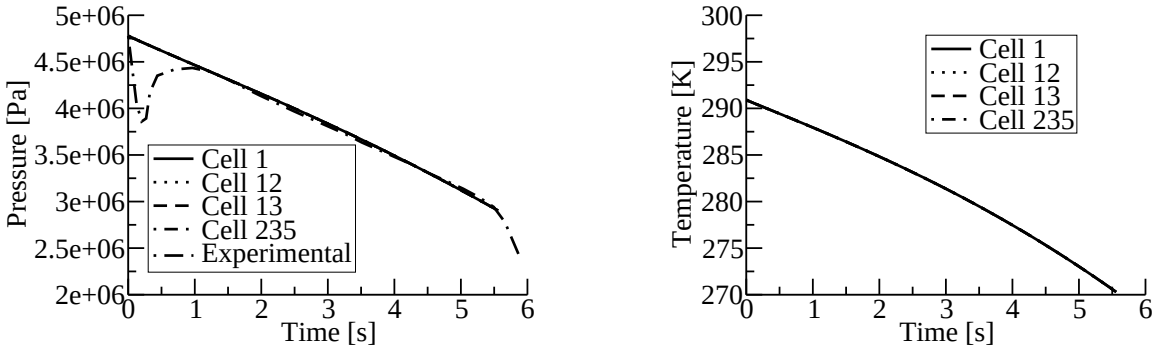

(a) Pressure

(b) Temperature

Figure 1: Pressure and temperature using Prince initial data

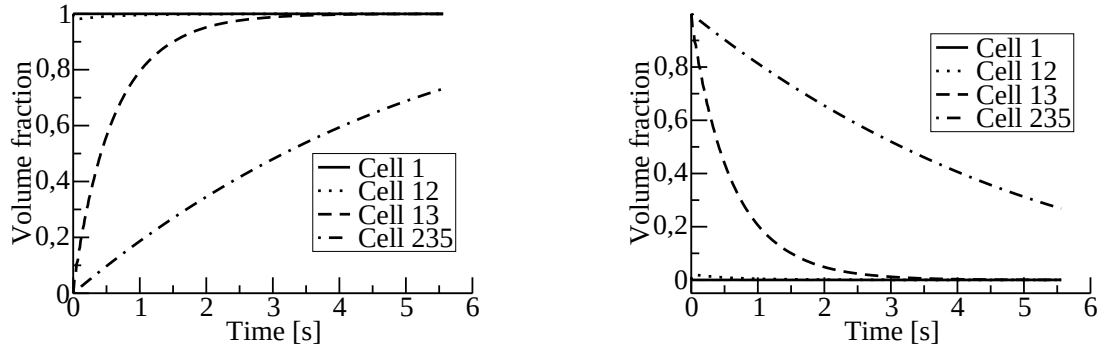

(a) Vapor volume fraction

(b) Liquid volume fraction

Figure 2: Volume fractions using Prince initial data

of the computation cell number 12 is the last cell that contains only vapor, cell number 13 is the first cell that contains only liquid and cell number 235 is placed at the outlet. Vapor volume fraction increases continuously in the cells that contained only liquid and has a small drop followed by an increase in the cells that contain only vapor and located near the cells that contain liquid. The reason is that the velocity computed at the beginning of the computation has a negative value in that cells. The mass of N_2O inside the tank at the beginning of the computation is 7.15 kg, with 7.08 kg for

DOI: 10.13009/EUCASS2019-229

the liquid phase. At the end of the computation there are 2.2 kg of liquid nitrous oxide and 0.57 kg of vapor. The mass flow rate decreases linearly with respect to time, this behavior can be observed also in the computations involving other initial conditions. The experimental final pressure value is 2.91 MPa, close to the value obtained in the computation. Prince[8] estimated a mean nitrous oxide mass flow rate of 0.819 kg/s and the value computed is 0.806 kg/s, so it is slightly lower.

4.2 Zilliac

Figures 3 and 4 represent results obtained using Zilliac's data set.[14] Pressure downstream of the injector is 1.0 MPa, a value measured in the experiment. The same observations done in Sec. 4.1 can be applied here to both pressure and temperature. At the beginning of the computation the last cell containing vapor is cell number 144, and the first cell containing liquid is cell 145. Volume fractions, plotted in Fig. 4, show the same trend outlined in Sec. 4.1. In this case the mass of liquid nitrous oxide in the tank at the beginning of the simulation is 18.48 kg and the mass of nitrous oxide vapor is 1.68 kg. At the end the mass of liquid is 3.78 kg and the mass of vapor is 2.49 kg. The amount of nitrous oxide that remains in the tank at the end of the computation, after 4.91 s, is higher than the experimental value as can be seen looking at Fig. 5. Moreover, looking again at Fig. 5, it is possible to notice that the mass in the tank decreases almost linearly with respect to time in the firsts five seconds of the experiment. This implies a nearly constant mass flow rate. The computed mass flow rate is not constant with respect to time, but it decreases linearly, with a mean value of 2.81 kg/s and is lower than the mean experimental mass flow rate. A reason for this is that the vapor volume fraction in the outlet cell is continuously increasing, as shown in Fig. 4(a) and this reduces the mass flow rate.

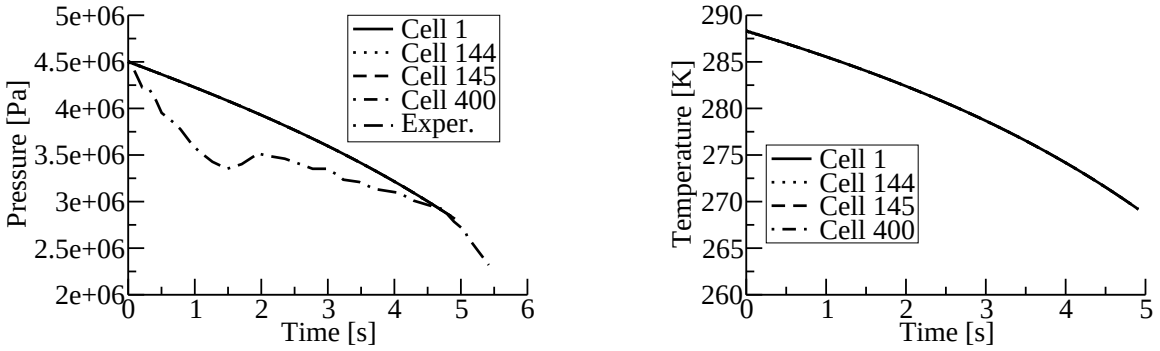

(a) Pressure (b) Temperature

Figure 3: Pressure and temperature using Zilliac's initial data

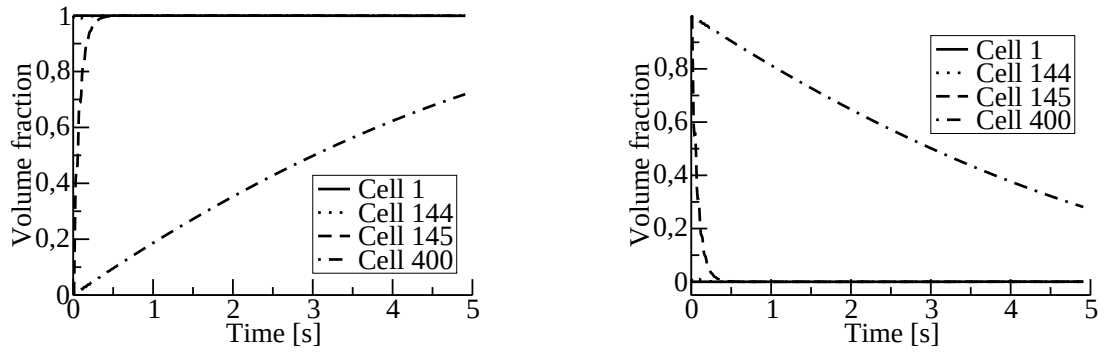

(a) Vapor volume fraction (b) Liquid volume fraction

Figure 4: Volume fractions using Zilliac's initial data

DOI: 10.13009/EUCASS2019-229

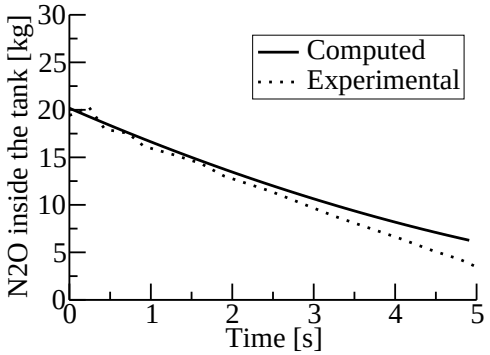

Figure 5: N_2O mass inside the tank using Zilliac's initial data

4.3 Zimmerman

Results obtained using Zimmerman's data set initial conditions[15] are shown in Figs. 6(a), 6(b) and 7, where Figs. 6(a) and 6(b) show the experimental pressure and temperature together with computed pressure and temperature. The same considerations done for pressure in Sec. 4.1 are still valid here and can be extended also to temperature, that has a trend similar to pressure, because the solution given by our model is in local thermodynamic equilibrium. At the beginning of the computation vapor is present in cells from 1 to 13, whereas cells from 14 to 100 contain liquid nitrous oxide. Volume fractions are plotted in Fig. 7 and the same conclusions for volume fractions presented in Sec. 4.1 can be applied here. At the beginning of the computation the quantity of nitrous oxide inside the tank is: $0.13\,kg$ for the liquid phase N_2O and $0.0025\,kg$ for the gas phase. At the end the amount of liquid is $0.042\,kg$ and the amount of vapor is $0.009\,kg$.

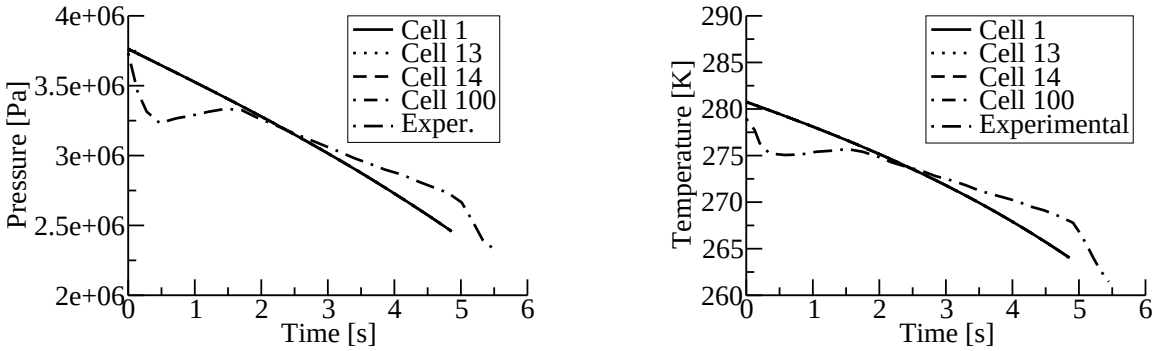

(a) Pressure

(b) Temperature

Figure 6: Pressure and temperature using Zimmerman's initial data

5. Conclusions

The results presented in this contribution with the multiphase model are similar to the results obtained using the equilibrium model,[15] because the infinite speed of relaxation of the source terms imposes locally both mechanical and thermodynamic equilibrium. However the multiphase model is preferable for the following reasons: 1) it allows both phases to be in all the computational domain, so the tank is not divided into two distinct parts one containing only liquid and the other containing only vapor, a fact that is not observed in the experiments; 2) thermodynamic equilibrium is imposed locally instead of globally; 3) it is possible to model tanks having two dimensional or three dimensional geometries without changes in the mathematical model; 4) phase transition is computed using the relaxation of chemical potential. The computed nitrous oxide mass inside the tank at the end of the computations is higher than the experimental value. The computed decrease in the mass flow rate leaving the tank is reasonably due to the continuous increment

DOI: 10.13009/EUCASS2019-229

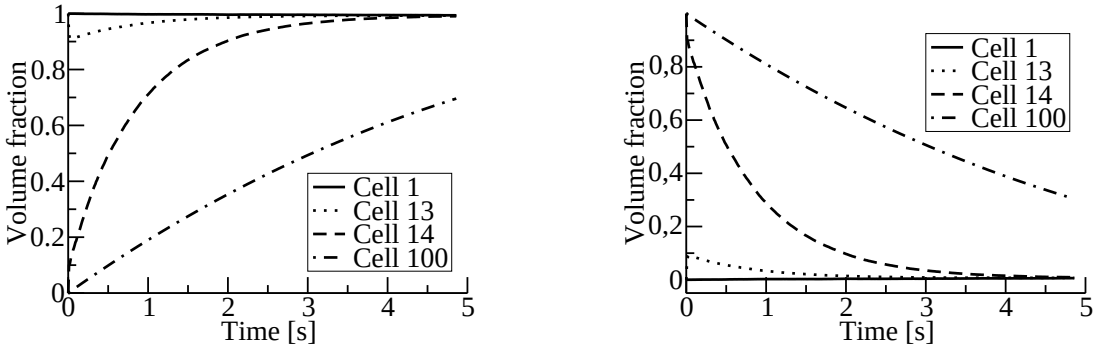

(a) Vapor volume fraction

(b) Liquid volume fraction

Figure 7: Volume fractions using Zimmerman's initial data

of vapor volume fraction in the outlet cell and this fact decreases the mixture density at the tank outlet.
Heat transfer from the tank to the walls and from the walls to ambient and the buoyancy effect of gravity can be easily added to the governing equations. The introduction of viscous stress tensor and heat flux and of a finite relaxation velocity of the source terms, instead of the infinite one used in this work, can improve significantly the model, allowing the liquid and the vapor phase to be in non equilibrium conditions and to have different pressure, temperature and velocity. This will allow the model to better approximate the initial pressure drop observed in tank draining experiments and to better estimate the amount of nitrous oxide left inside the tank.

References

[1] Nist database. `https://webbook.nist.gov/chemistry/`. Accessed: 30-5-2019.

[2] M.R. Baer and J.W. Nunziato. A two-phase mixture theory of the deflagration-to-detonation transition (DDT) in reactive granular materials. *Int. J. Multiphase Flows*, 12:861–889, 1986.

[3] J. Dyer, E. Doran, Z. Dunn, and K. Lohner. Modeling feed system flow physics for self-pressurizing propellants. *43rd AIAA/ASME/SAE/ASEE Joint propulsion Conference and Exhibit*, AIAA paper 2007-5702, 2007.

[4] E. Han, M. Hantke, and S. Müller. Modeling of multi-component flows with phase transition and application to collapsing bubbles. Technical Report 409, IGPM, Aachen, 2014.

[5] E. Han, M. Hantke, and S. Müller. Efficient and robust relaxation procedures for multi-component mixtures including phase transitions. *Journal of Computational Physics*, 338:217–239, 2017.

[6] S. Müller, M. Hantke, and P. Richter. Closure conditions for non-equilibrium multi-component models. *Contin. Mech. Thermodyn.*, 28:1157–1189, 2016.

[7] O. Le Métayer and R. Saurel. The Noble-Abel stiffened-gas equation of state. *Physics of Fluids*, 28:046102, 2016.

[8] E.R. Prince, S. Krishmanoorth, I. Ravlich, A. Kotine, A.C. Fickes, A.I. Fidalgo, K. Freeman, K. Anderson, and D. Gerson. Design, analysis, fabrication, ground-test and flight of a two-stage hybrid and solid rocket. *49th AIAA/ASME/SAE/ASEE Joint Propulsion Conference and Exhibit*, AIAA paper 2013-4105, 2013.

[9] R. Saurel and R. Abgrall. A multiphase Godunov method for compressible multifluid and multiphase flows. *Journal of Computational Physics*, 150:425–467, 1999.

[10] B.J. Solomon. *Engineering Model to calculate Mass Flow Rate of a Two-Phase Saturated Fluid Through an injector Orifice*. PhD thesis, Utah State University, 2011.

[11] G. Strang. On the construction and comparison of difference schemes. *SIAM J. Numer. Anal.*, 5:506–517, 1968.

[12] E. F. Toro. *Riemann Solvers and Numerical Methods for Fluid Dynamics: A Practical Introduction*. Springer, Berlin, 1997.

DOI: 10.13009/EUCASS2019-229

[13] A. Zein. *Numerical methods for multiphase mixture conservation laws with phase transition*. PhD thesis, Otto-von-Guericke-Universität, Magdeburg, 2010.

[14] G. Zilliac and M.A. Karabeyoglu. Modeling of propellant tank pressurization. *41st AIAA/ASME/SAE/ASEE joint Propulsion Conference and Exhibit*, AIAA paper 2005-3549, 2005.

[15] J.E. Zimmerman, B.S. Waxman, and B.J. Cantwell. Review and evaluation of models for self-pressurizing propellant tank dynamics. *49th AIAA/ASME/SAE/ASEE Joint Propulsion Conference*, AIAA paper 2013-4045, 2013.